Deletion of NFIX results in defective progression through meiosis within the mouse testis†

Authors: Davila, Raul Ayala, Spiller, Cassy, Harkins, Danyon, Harvey, Tracey, Jordan, Philip W., et al.

Source: Biology of Reproduction, 106(6) : 1191-1205

Published By: Society for the Study of Reproduction

URL: https://doi.org/10.1093/biolre/ioac049

Biology of Reproduction, 2022, **106(6)**, 1191–1205
https://doi.org/10.1093/biolre/ioac049
Advance access publication date 3 March 2022
Research Article

Deletion of NFIX results in defective progression through meiosis within the mouse testis†

Raul Ayala Davila[1], Cassy Spiller[1], Danyon Harkins[1], Tracey Harvey[1], Philip W. Jordan[2], Richard M. Gronostajski[3], Michael Piper[1,4,‡,*] and Josephine Bowles[1,5,‡,*]

[1]School of Biomedical Sciences, The University of Queensland, Brisbane, Australia
[2]Department of Biochemistry and Molecular Biology, Johns Hopkins University Bloomberg School of Public Health, Baltimore, MD, USA
[3]Department of Biochemistry, Program in Genetics, Genomics and Bioinformatics, Center of Excellence in Bioinformatics and Life Sciences, State University of New York at Buffalo, Buffalo, NY, USA
[4]Queensland Brain Institute, The University of Queensland, Brisbane, Australia
[5]Institute for Molecular Bioscience, The University of Queensland, Brisbane, Australia

*__Correspondence__: School of Biomedical Sciences, The University of Queensland, Brisbane 4072, Australia.
Tel: +61733653056; E-mail: jo.bowles@uq.edu.au; (Josephine Bowles) Tel: +61733469873; E-mail: m.piper@uq.edu.au (Michael Piper)

†__Grant Support__: This work was supported by Australian Research Council Discovery Project grants to MP (DP180100017) and to JB (DP180103811 and DP200102896). RAD and DH were supported by Australian Government Research Training Program Scholarships.

‡These authors contributed equally to this work.

Abstract

Members of the nuclear factor I (NFI) family are key regulators of stem cell biology during development, with well-documented roles for NFIA, NFIB, and NFIX in a variety of developing tissues, including brain, muscle, and lung. Given the central role these factors play in stem cell biology, we posited that they may be pivotal for spermatogonial stem cells or further developing spermatogonia during testicular development. Surprisingly, in stark contrast to other developing organ systems where NFI members are co-expressed, these NFI family members show discrete patterns of expression within the seminiferous tubules. Sertoli cells (spermatogenic supporting cells) express NFIA, spermatocytes express NFIX, round spermatids express NFIB, and peritubular myoid cells express each of these three family members. Further analysis of NFIX expression during the cycle of the seminiferous epithelium revealed expression not in spermatogonia, as we anticipated, but in spermatocytes. These data suggested a potential role for NFIX in spermatogenesis. To investigate, we analyzed mice with constitutive deletion of *Nfix* (*Nfix*-null). Assessment of germ cells in the postnatal day 20 (P20) testes of *Nfix*-null mice revealed that spermatocytes initiate meiosis, but zygotene stage spermatocytes display structural defects in the synaptonemal complex, and increased instances of unrepaired DNA double-strand breaks. Many developing spermatocytes in the *Nfix*-null testis exhibited multinucleation. As a result of these defects, spermatogenesis is blocked at early diplotene and very few round spermatids are produced. Collectively, these novel data establish the global requirement for NFIX in correct meiotic progression during the first wave of spermatogenesis.

Summary Sentence

The transcription factor NFIX is required for meiotic progression during the first wave of spermatogenesis in the mouse.

Received: November 20, 2022. **Revised:** January 17, 2022. **Accepted:** February 24, 2022

Graphical Abstract

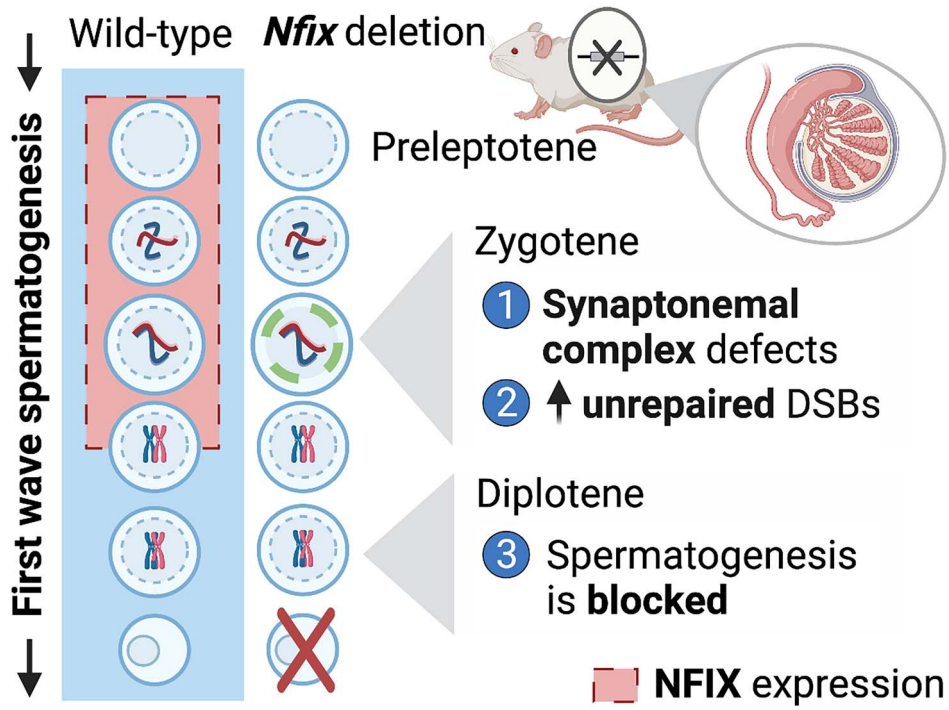

Keywords: NFI, NIFX, meiosis, meiotic progression, spermatogenesis, first wave of spermatogenesis

Introduction

Male infertility is surprisingly common and, although not life-threatening, is associated with substantial emotional suffering and financial costs. About 8–12% of couples of reproductive age are infertile, and in at least half of these cases, the problem is male factor infertility [1]. Spermatogenesis, the development of mature functional haploid sperm from diploid spermatogonial stem cells, begins at puberty and continues throughout life. Sperm production is a highly complex, multistep developmental process that occurs within the seminiferous epithelium of the testis tubules. The seminiferous tubules are comprised of Sertoli or "nurse" cells, which support the complete, stepwise development of the male germ line, from the spermatogonial stem cells (SSCs), spermatogonia, spermatocytes, through to elongated spermatids. Because sperm development occurs over several weeks, and is an asynchronous process (i.e., the stem cells begin differentiating at different times), a cross-section through adult testis reveals tubules with different combinations of the differentiating germinal cell types [2]. The only exception to this asynchrony is during the initial round of spermatogenesis in mice, in which differentiation is triggered in a largely synchronous manner in all tubules shortly after birth.

SSCs are responsible for the extraordinary feat of producing copious numbers of differentiated sperm throughout life. As well as undergoing self-renewal, SSCs produce progenitor cells (spermatogonia) that undergo multiple mitotic divisions before initiating meiosis, the reductive form of cell division that is unique to the germ line, and which results in the production of haploid sperm. Meiosis is supported in situ by the somatic Sertoli cells. During meiosis, chromosomal recombination occurs, with this genomic shuffling ensuring that every gamete produced is unique; as such, meiosis is not only necessary for production of haploid gametes but is also essential for evolution. Because gamete quality is of paramount importance, there are multiple mechanisms by which defective germline cells are eliminated, particularly if they fail to progress through meiosis (reviewed by [3]). Critically, our understanding of the molecular mechanisms regulating meiotic progression remains limited, and unexplained meiotic arrest underlies many cases of male infertility.

Members of the Nuclear Factor I (NFI) family of transcription factors are encoded by four closely related genes, *Nfia*, *Nfib*, *Nfic*, and *Nfix*. NFI proteins are involved in a diverse range of developmental processes [4, 5] with NFIA, NFIB, and NFIX proving particularly important for regulating stem cell behavior, including the balance between cellular proliferation and differentiation in the developing brain [6–8] and skeletal muscles [9]. NFI proteins share a conserved DNA binding/dimerization domain at their N-termini and a C-terminal transactivation/repression domain that is highly variable due to alternative splicing [10, 11]. NFI proteins homo- or heterodimerize to allow strong binding to the palindromic consensus sequence 5′-TGGCA-($N_{3–5}$)-TGCCA-3′ or weaker binding to half sites, and are able to induce either activation or repression of target genes in a cell-type and promoter-specific manner [10, 12–14].

We, and others, have previously examined expression and function of NFI proteins within the murine nervous system; one common theme arising from these studies has been that NFIA, NFIB, and NFIX share highly similar expression patterns within neural stem cells [15]. For example, within the

developing cerebral cortex, NFIA, NFIB, and NFIX are all expressed by neural progenitor cells [8, 16, 17]. Similarly, granule neuron progenitor cells within the nascent postnatal cerebellum, neural progenitor cells within the embryonic spinal cord, and progenitor cells within the neural retina co-express these NFI family members, as do adult neural progenitor cells within the hippocampal dentate gyrus [18–21]. At a functional level, the fact that similar neural phenotypes are observed in individual *Nfi* knockout mouse models also hints at shared roles in regulating development of the nervous system [20, 22, 23]. Given the strong, convergent evidence for related and possibly redundant roles for NFI family members in regulating neural progenitor cell activity during development, we hypothesized that members of this family may play a similar role in the testis, where stem cells are critical for the ongoing production of sperm. Surprisingly, in contrast to this hypothesis, we revealed limited overlap of expression of NFIA, NFIB, and NFIX within the juvenile and adult testis and demonstrated that NFIX was the only family member expressed in spermatocytes during postnatal life. Although we did not detect NFIX in spermatogonia, we did find that NFIX was important for normal spermatogenesis: constitutive deletion of *Nfix* culminated in aberrant meiosis and the absence of round spermatids at P20. Collectively, this study reveals previously unrecognized cell-type specific expression patterns of NFIs within the testis and establishes the global requirement for NFIX in correct meiotic progression during the first wave of spermatogenesis.

Results

NFIs show distinct patterns of expression within the adult testis

To examine the expression of NFIA, NFIB, and NFIX within the adult testis, we performed co-immunofluorescent labeling of these factors alongside the cell-type specific markers TRA98 (germ cell marker) and SOX9 (Sertoli cell marker), followed by imaging using confocal microscopy. Our analysis revealed an unexpectedly discrete pattern of NFI protein expression. NFIA was expressed by Sertoli cells, peritubular myoid cells lining the seminiferous tubules, and cells in the interstitial space of the testis (Supplementary Figure S1A–D). In contrast, NFIB was detected in cells of the interstitial space, as well as peritubular myoid cells and round spermatids, but was absent from Sertoli cells (Supplementary Figure S1E–H). Finally, NFIX expression was evident within germ cells, as well as within cells in the interstitial space and peritubular myoid cells, but not within Sertoli cells (Supplementary Figure S1I–L). Due to unavailability of suitable antibodies for NFIC, we were unable to assess its expression pattern during testis development. However, we have investigated the expression of *Nfic* by reanalyzing single cell RNA sequencing (RNA-seq) data from three recent studies [24–26]. Here we found that *Nfic* mRNA is expressed by spermatogonia, Leydig, and Sertoli cells in adult testis (Supplementary Figure S2). These data also indicate that expression we detect in the interstitial space, for each of NFIA, NFIB, and NFIX, may reflect expression in Leydig cells. These data suggest that, unlike stem cells within the nervous system that co-express these factors, spermatocytes express NFIX, but not NFIA or NFIB, within the adult testis.

NFIA and NFIX are expressed by Sertoli and germ cells, respectively, in both juvenile and adult testes

Germ cells and Sertoli cells are the only cells present within the seminiferous tubules, acting coordinately to ensure successful and efficient spermatogenesis. Having determined that NFIA and NFIX are expressed in the adult testis by Sertoli and germ cells, respectively, we next sought to determine whether this nonoverlapping expression was also evident during the distinctive first round of spermatogenesis by examining postnatal day (P) 20 testes. Using nuclear shape and cellular position as a guide (via DAPI staining), we could reliably identify both Sertoli cells and germ cells. Critically, in both P20 (Figure 1A and B) and adult (Figure 1C and D) testes we found that Sertoli cells expressed NFIA, but not NFIX, and that only NFIX was expressed by germ cells. Consistent with our initial observations (Supplementary Figure S1), peritubular myoid cells, which are located external to the testicular tubules, expressed both NFIA and NFIX. Collectively, these novel data indicate that members of the NFI family display discrete patterns of expression within the juvenile and adult testis, and that NFIX and NFIA expression patterns are mutually exclusive in the important germ and Sertoli cell populations. Expression of NFIX in the germ cells suggests that it may have a role regulating germ cell differentiation and spermatogenesis within both the postnatal and adult testis.

NFIX is expressed in the germline during a defined window of spermatogenesis

In the mammalian testis, the epithelium of the seminiferous tubules undergoes repetitious rounds of spermatogenesis known as the cycle of the seminiferous epithelium. Traditionally, the epithelium cycle has been subdivided into 12 stages in mice [27] such that in any cross section of a seminiferous tubule, 1 of 12 possible "cellular associations" will be observed, indicating the "stage" of the seminiferous cycle at that point in the tubule (Figure 2G, adapted from [2]). Having discovered that NFIX was expressed in some germ cells in both P20 and adult testes, we sought to determine the precise pattern of NFIX expression within the seminiferous cycle. As described previously [2], we divided the 12 stages into three groups: Stages I–V as "early"; Stages VI–VIII as "middle"; and Stages IX–XII as "late" (Figure 2). We performed co-immunofluorescent labeling for NFIX and phosphorylated histone H2AX (γH2AX), a marker of the DNA double strand breaks that are crucial for recombination and pairing between homologous chromosomes and are first observed diffusely in the nucleus at the preleptotene stage, before becoming restricted to the XY body in pachytene [28]. We also used 4′,6-diamidino-2-phenylindole (DAPI) staining to identify the stage and maturity of cells within the seminiferous cycle. The earliest expression of NFIX that we could detect was in preleptotene (pl) spermatocytes, at stage VII/VIII. NFIX remained in germ cells as they progressed through meiosis, with NFIX protein detected at leptotene (L), zygotene (Z), and early pachytene (P) spermatocyte stages (Supplementary Figure 2A–F). NFIX was not detectable in the more mature pachytene spermatocytes present in middle and late cellular association stages. Taken together these results suggest that, although NFI family members are often associated with stem cell function in somatic systems, NFIX is not expressed in spermatogonia, but is observed in more differentiated stages in the germline.

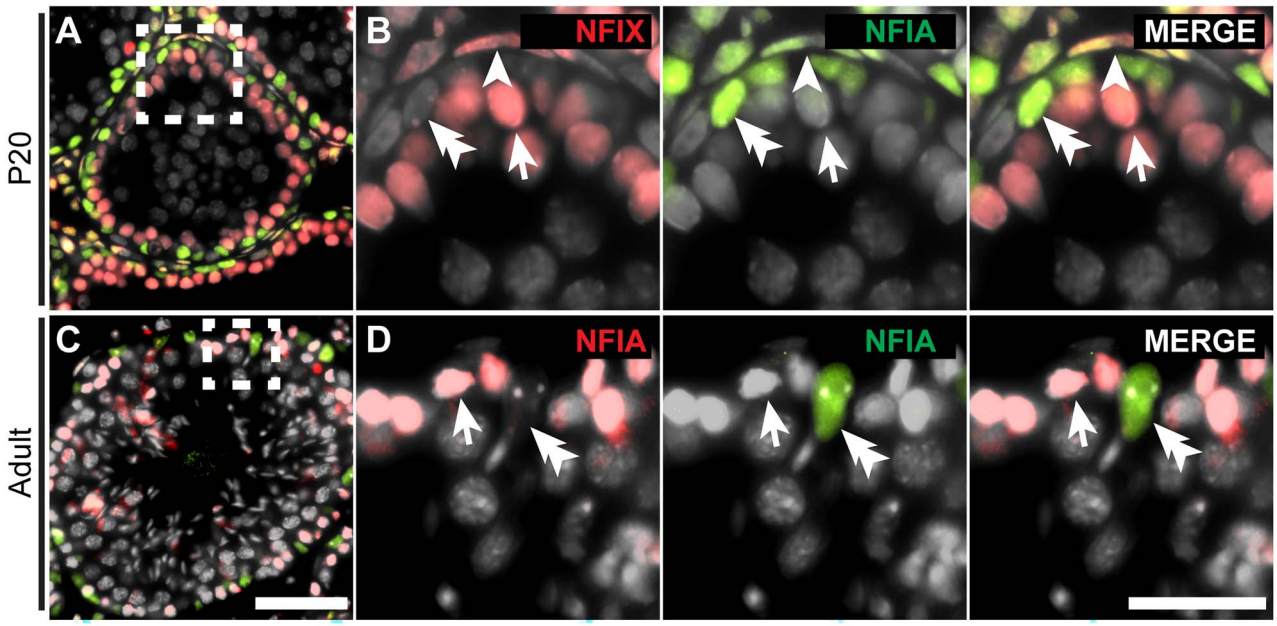

Figure 1. Nonoverlapping expression of NFIA and NFIX by germ cells within the first wave of spermatogenesis (P20) and adult seminiferous tubules. (*A*, *C*) Cross section of the seminiferous tubules from P20 (*A*) and adult (*C*) testes. Dashed boxes indicate a representative region, shown at higher magnification to the right in *B* and *D*, respectively. DAPI was used to visualize the cell nucleus (gray). (*A*, *B*) Immunofluorescent labeling of NFIA (green) and NFIX (red) within the P20 testis. Within the seminiferous tubules germ cells expressed NFIX (arrow in *B*) while Sertoli cells expressed NFIA (double arrowhead in *B*), while cells lining the tubules (peritubular myoid cells; arrowhead in *B*) were positive for both NFIX and NFIA. (*C*, *D*) In the adult testis, the expression of these transcription factors was also nonoverlapping, with NFIA expression evident within Sertoli cells (double arrowheads in *D*) and NFIX expression evident within germ cells (arrows in *D*). $n = 3$. Scale bars: in *A*, *C* = 50 μm; *B*, *D* = 25 μm.

Gross morphology, including testis size, is reduced in *Nfix*-null mice

Given the expression of NFIX in pre-leptotene through to early pachytene spermatocytes, we hypothesized that this transcription factor might play an important role during meiosis. To investigate this, we analyzed mice with a constitutive targeted disruption of the DNA-binding domain region of *Nfix* [29]. Mice lacking *Nfix* exhibit a range of phenotypes, including a marked reduction in body size and hydrocephalus, and survive only until ~P22 [30]: for this reason, we were only able to investigate the unique first round of spermatogenesis in the absence of *Nfix*. As expected, P20 mice lacking *Nfix* were smaller, and exhibited a domed skull indicative of hydrocephalus (Figure 3A). *Nfix*-null mice had significantly smaller testis measurements (Figure 3B, C, F, and G); however, these were proportional to overall body size because testis/body weight ratio was similar between *Nfix*-null mutants and controls (Figure 3E).

In the absence of *Nfix,* germ cells in the testis are blocked in prophase of meiosis I

We next assessed germ cell development in the *Nfix* mutant males, examining hematoxylin-stained paraffin sections of P20 testes. In wild-type mice we observed normal spermatogenesis that included cell types ranging from spermatogonia through to round spermatids (the most mature spermatogenic cells expected at this developmental age; Figure 4A–C). In contrast, testis sections from *Nfix*$^{-/-}$ mice revealed a range of abnormalities, the most striking being the presence of many aberrant multinucleated giant cells (termed "symplasts") [31] (Figure 4D–F). Quantification of germ cell stages also revealed an almost complete absence of round spermatids within *Nfix*-null tubules (Figure 4G). In line with smaller testis size and the almost complete lack of round spermatids, tubule diameter was also significantly reduced in mutant mice in comparison to wild-type controls (Figure 4H). These observations suggest that most spermatocytes in postnatal testes of *Nfix*-null mice are blocked during meiosis, prior to the formation of round spermatids. To determine how far through meiosis, I the *Nfix*-null germ cells progressed we analyzed expression of α-tubulin, which can be used as a proxy for microtubule assembly due to specific distributions during pachytene/diplotene and metaphase (Supplementary Figure S3G). We observed α-tubulin filaments in the cytoplasm and at the nuclear periphery throughout meiotic prophase I, in both wild-type and *Nfix*-null cells (Supplementary Figure S3A–F). In the wild-type, we also observed cells with α-tubulin positive spindle poles, indicative of cells in metaphase (Supplementary Figure S3A–D). However, we did not observe any cells with α-tubulin positive spindle poles in the mutant, suggesting that *Nfix*-null spermatocytes do not reach metaphase.

Some zygotene spermatocytes in *Nfix*-null testes exhibited highly abnormal SYCP3 localization and no cells progressed beyond early diplotene

Having determined that *Nfix*-null germ cells do not reach metaphase of meiosis I, we next assessed progression from leptonema through to zygonema. We visualized the presence and localization of synaptonemal complex protein (SYCP1) and SYCP3, which are two key markers of the synaptonemal complex (SC). SYCP3 is a structural component of the

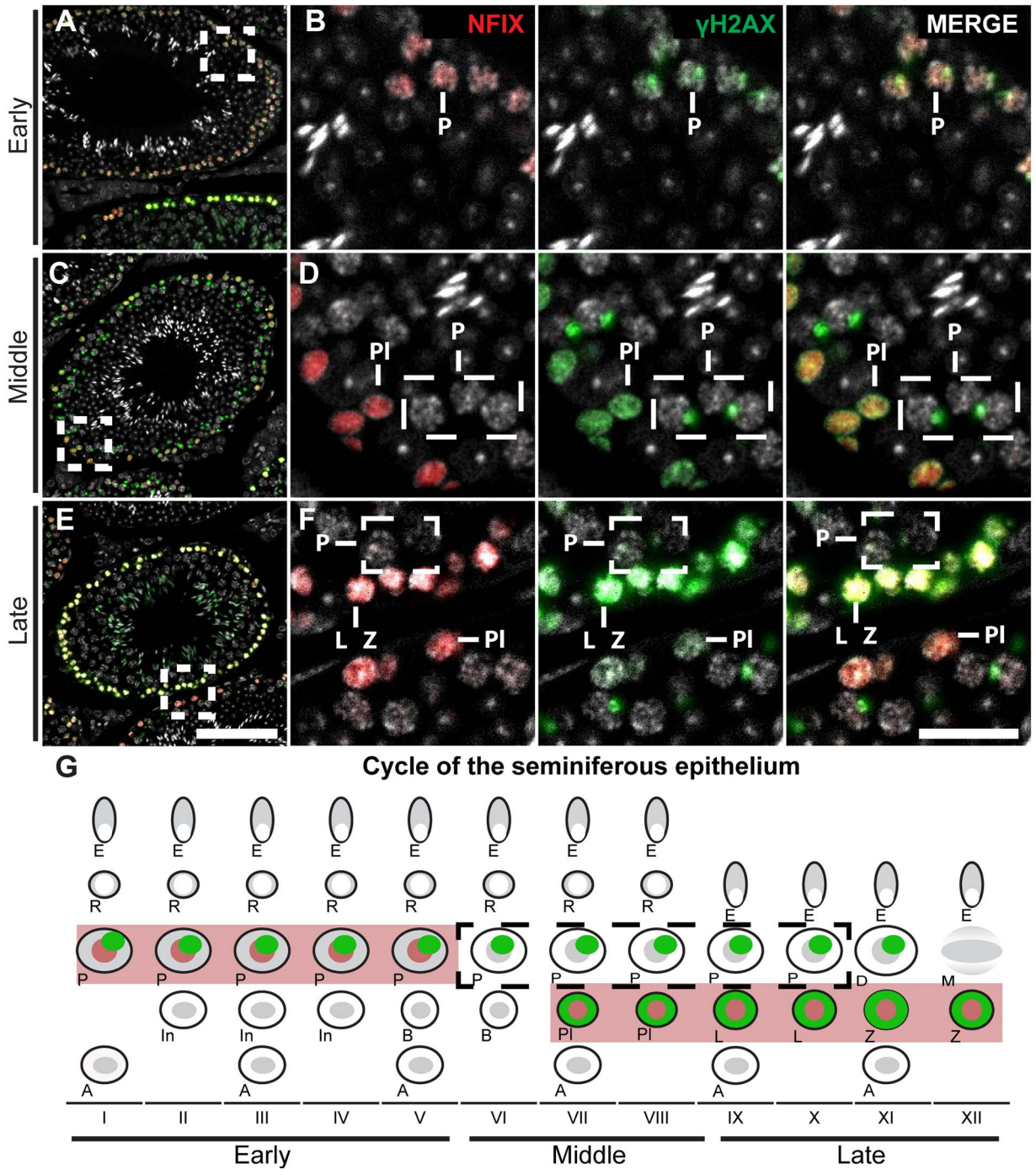

Figure 2. Preleptotene, leptotene, zygotene, and early pachytene spermatocytes express NFIX. Cross section of the seminiferous tubules from an adult testis. The boxed regions in *A*, *C*, and *E* are shown at higher magnification in *B*, *D*, and *F*, respectively. Immunofluorescent labeling of NFIX (red), γH2AX (green), and DAPI (gray) are shown at Early (*A*, *B*), Middle (*C*, *D*), and Late (*E*, *F*) stages of the epithelial cycle in the adult testis. (*A*, *B*) Representative cross section of the seminiferous tubule in the "Early stage" which is characterized by a complete absence of preleptotene and leptotene spermatocytes. Early pachytene (P) spermatocytes express NFIX at this stage. Note the specialized nuclear territory known as the XY body (γH2AX, green). (*C*, *D*) Representative cross section of the seminiferous tubule in the "Middle" stage. Preleptotene (Pl) spermatocytes are round and visible close to the basement membrane, are γH2AX positive, and are characterized by a small nucleus with some heterochromatic clumps. These preleptotene spermatocytes express NFIX. Pachytene (P) spermatocytes do not express NFIX at this stage (dashed boxes in D). (*E*, *F*) Representative cross-section of the seminiferous tubule in the "Late" stage. The stage is characterized by a complete absence of round spermatids. Leptotene (L) and zygotene (Z) spermatocytes are present and are γH2AX positive; these cells also express NFIX. Pachytene spermatocytes do not express NFIX at this stage (dashed boxes in *F*). Note that panel F shows adjacent tubules, one in "Late" stage (top) and the second in the "Middle" stage (bottom). (*G*) Schematic of the cycle of the seminiferous epithelium. Stages were considered in three groups: Stage I–V as Early; Stages VI–VIII as Middle; and Stages IX–XII as Late. Expected expression and localization of γH2AX is shown in green; γH2AX is initially diffusely localized in pre-leptotene, leptotene, and zygotene stages and then localized to the XY body at pachytene and diplotene stages (depicted by small green dots). The cell types that express

axial/lateral elements that form along each chromosome homolog and is detectable at leptonema. SYCP1 is the main constituent of the transverse elements, first detectable in regions of chromosome pairing (synapsis) at zygonema [32–34]. At the diplotene stage the SC disassembles, but homologues remain attached at cross-over points, and SYCP1 dissociates while SYCP3 remains attached [35]. In P20 wild-type and *Nfix*-null samples we were able to identify spermatocytes in leptotene (SYCP3 marking the axes of chromosomes in a thread-like pattern (Figure 5A and B)). In P20 wild-type samples we identified classical zygotene spermatocytes, in which synapsis and the formation of the SC had occurred (SYCP3 and SYCP1, a transverse filament marker, seen in proximity, Figure 6C). In *Nfix*-null zygotene spermatocytes, the extensive network of fine SYCP3 threads was not as closely associated with SYCP1, suggesting a delay or defect in SC formation (Figure 5D). In addition, we detected abnormal zygotene cells displaying large aggregates of SYCP3 close to the nuclear envelope (Figure 5E). These abnormal zygotene cells were readily identifiable in just over 50% of zygotene-containing tubules (Supplementary Figure S4A). Despite finding these abnormalities in the *Nfix*-null samples, the proportion of tubules scored as containing apparently normal pachytene spermatocytes (SC extended along the full length of all chromosomes, SYCP1 and SYCP3 overlapping) were similar in wild-type and *Nfix*-null samples (Figures 5F and G, Supplementary Figure S4B). Further, diplotene spermatocytes (chromosomes beginning to separate as the SC disassembles), comparable to wild-type, were observed in *Nfix*-null paraffin sections (Figures 5H and I, Supplementary Figure S4C). However, no cells in diakinesis (SC disassembly is complete, no SYCP1, chromosomes completely separated) were found in *Nfix*-null sections (Figures 5J, Supplementary Figure S4D). We further visualized phosphorylated histone H3 (PH3), which marks chromosome condensation characteristic of the pachynema to diplonema transition [36, 37]. As expected, PH3 was first detected at early/mid diplonema in wild-type samples, but this marker was not observed in the *Nfix*-null samples (Figure 5K–N). This result indicates that meiosis I chromosomes did not reach, or were unable to undergo, condensation and progress beyond early diplonema in the absence of NFIX.

Spermatocytes exhibit increased rates of apoptosis during the first round of spermatogenesis in *Nfix*-null testes

During our SYCP1 and SYCP3 immunofluorescence analysis (Figure 5) we noted what appeared to be an increase in apoptotic cells in the *Nfix*-null mutant samples (Supplementary Figure S4E), characterized by diffuse SYCP3 staining. We quantified the number of apoptotic cells per tubule, using the TUNEL assay: TUNEL-positive cells were found at a rate six times higher in P20 testes from *Nfix*-null mice compared with wild-type, where apoptotic cells were observed at a rate of less than 1 positive cell per tubule (Figure 6).

Formation of double-strand breaks and XY body appears normal in *Nfix*-null spermatocytes

Having discovered that some spermatocytes display abnormal zygotene morphology with respect to SYCP3 staining, and that diakinesis failed to occur in *Nfix*-null germ cells at P20, we next examined whether double-strand breaks (DSBs) form normally during the substages of prophase I of meiosis. We examined P20 testis sections for the presence and localization of γH2AX (a marker of DSBs that is actively induced in meiosis I and required for meiotic recombination) [28]. In wild-type mice, DSBs are identified by weak, diffuse γH2AX staining at the preleptotene and leptotene stages and this staining becomes localized to nuclear foci in zygotene and early pachytene-stage spermatocytes. Following DSB repair on the autosomes, γH2AX becomes localized to the XY body (in a peripheral nuclear subdomain) in mid- to late pachytene (Supplementary Figure S5) [38]. We observed normal localization of γH2AX in the *Nfix*-null testes in pre-leptotene, zygotene, pachytene, and diplotene cell types in comparison to controls (Supplementary Figure S5B–O). These data indicate that DSB formation and resolution, and XY body formation, appears to occur normally in the absence of NFIX.

Accumulation of RAD51 foci along axial/lateral elements of the synaptonemal complex is retained in *Nfix*-null spermatocytes

Our analysis of γH2AX expression (Supplementary Figure S5) revealed DSBs were occurring in the absence of *Nfix*, so we next sought to investigate to what extent subsequent homologous recombination was occurring. Homologous recombination is essential to ensure correct segregation of chromosomes at the first meiotic division and is mediated by RAD51 and DMC1 recombinases. These recombinase proteins load onto the single-stranded DNA produced at the end of the DSBs, forming a nucleoprotein complex that drives homology search and strand invasion, thus initiating recombination between homologous chromosomes (reviewed by [39]). Immunostaining of testis sections for RAD51 revealed significantly more RAD51 foci in zygotene stage *Nfix*-null spermatocytes, compared to controls (Figure 7B, D and F): this was true for zygotene cells that were relatively normal looking (Figure 7D), as well as for the abnormal cells characterized by SYCP3 clumps at the nuclear periphery (Figure 7F). We found an average of 56.57 ± 8.3 RAD51 foci in control zygotene spermatocytes, but an average of 102.1 ± 7.53 such foci per *Nfix*-null zygotene spermatocyte (Figure 7G). Similarly, pachytene spermatocytes in the *Nfix*-null testes showed intense RAD51 staining compared to that observed in the control (Figure 7C; cells at the center of the tubule). Normally RAD51 foci disappear from axial elements by the end of pachynema, only remaining in association with the sex chromosomes or in regions of failed synapsis in autosomes [40]. Thus, the retention of RAD51 in the *Nfix*-null spermatocytes may result from a high level of abnormal homologous recombination: it is possible that this contributes to the high level of apoptosis documented above (Figure 6).

Figure 2. NFIX are shown in the red shaded rectangle. Middle and Late stages of pachytene spermatocytes are enclosed by dashed boxes in both the fluorescence images and in the schematic. $n = 3$. Scale bars: *A*, *C*, *E* = 100 μm; *B*, *D*, *F* = 25 μm. Abbreviations: (A) spermatogonia cells, (In) intermediate spermatogonia cells, (B) B spermatogonia cells, (Pl) preleptotene spermatocytes, (L) leptotene spermatocytes, (Z) zygotene spermatocytes, (P) pachytene spermatocytes, (D) diplotene spermatocyte, (M) metaphase, (R) round spermatids, (E) elongated spermatids.

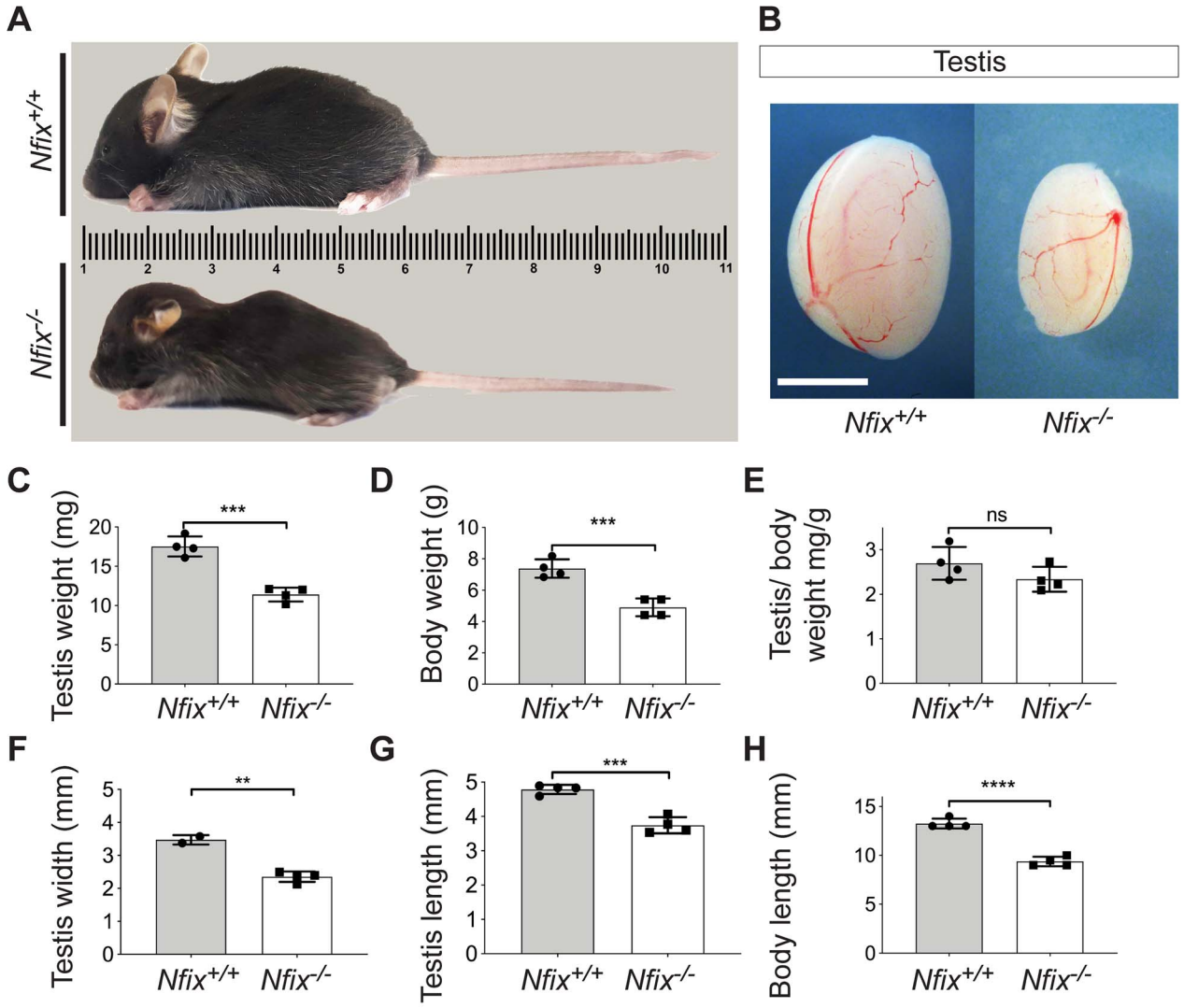

Figure 3. Testis size and body size were reduced in *Nfix*-null mice. (*A*) Lateral view of P20 $Nfix^{+/+}$ and $Nfix^{-/-}$ mice. $Nfix^{-/-}$ mice were smaller and exhibited a hunched back and a domed head shape. (*B*) Testicular morphology of wild-type ($Nfix^{+/+}$) versus *Nfix*-null ($Nfix^{-/-}$) mice. Testes were dissected from P20 $Nfix^{+/+}$ and $Nfix^{-/-}$ mice and were inspected macroscopically. Note the reduction in testicular size in the mutant (right). (*C–H*) Bar plots showing mean testis weight (C), body weight (D), and ratio of testis of body weight (E), as well as testis width (*F*), length (*G*), and body length (*H*) of $Nfix^{+/+}$ and $Nfix^{-/-}$ mice. There were significant reductions of testis width, length, and weight of $Nfix^{-/-}$ mice compared with the control. However, testis/body weight was not significantly different between $Nfix^{+/+}$ and $Nfix^{-/-}$ mice. Body length (*H*) was also significantly reduced in $Nfix^{-/-}$ mice. $n = 4$ for each genotype. Scale bar, 2000 μm. Error bars indicate SD, Students *t*-test, $^{**}P < 0.01$, $^{***}P < 0.001$ and $^{****}P < 0.0001$, ns = not significant.

Discussion

Based on what has been observed in other developmental systems, we hypothesized that NFI transcription factors might play important roles in mammalian testis development and/or spermatogenesis, particularly with respect to regulation of the proliferation/differentiation balance in spermatogonia. We found that NFIA, NFIB, and NIFX are indeed expressed in the mouse postnatal testis, but we were surprised to find that there was little co-expression of family members; this finding is in contrast to the overlapping expression patterns that is more commonly observed in other organs [41]. There are only two cell types within the testicular tubules, the Sertoli cells and the germ cells, and we found that NFIA, NIFB, and NFIX were expressed in discrete populations: NFIA in Sertoli cells, NFIX in spermatocytes and NFIB in a polarized region in round spermatids. Given the association of NFI family members with stem and progenitor cells in other systems, we were surprised to find that NFIX is not observed in spermatogonia. Instead, we found NFIX to be predominantly expressed from pre-leptotene up until early-pachytene stages of meiosis I. Outside of the testicular tubules, NFIA, NFIB and NFIC were also apparently expressed by some interstitial cells (Supplementary Figure S1). Although such expression would be consistent with transcriptomic data (Supplementary Figure S2), we note that nonspecific staining in the interstitial region of the adult testis is commonly observed (e.g., Supplementary Figure S6).

Analyzing a constitutively deleted *Nfix* mouse model [29], we found that global loss of *Nfix* impaired the initial pubertal round of spermatogenesis. Compared with adult rounds of spermatogenesis, the first round is largely synchronized, with each more differentiated spermatogonial cell type appearing in an orderly and regular stereotypical manner, thereby allowing more clarity in the analysis of any spermatogenic defects.

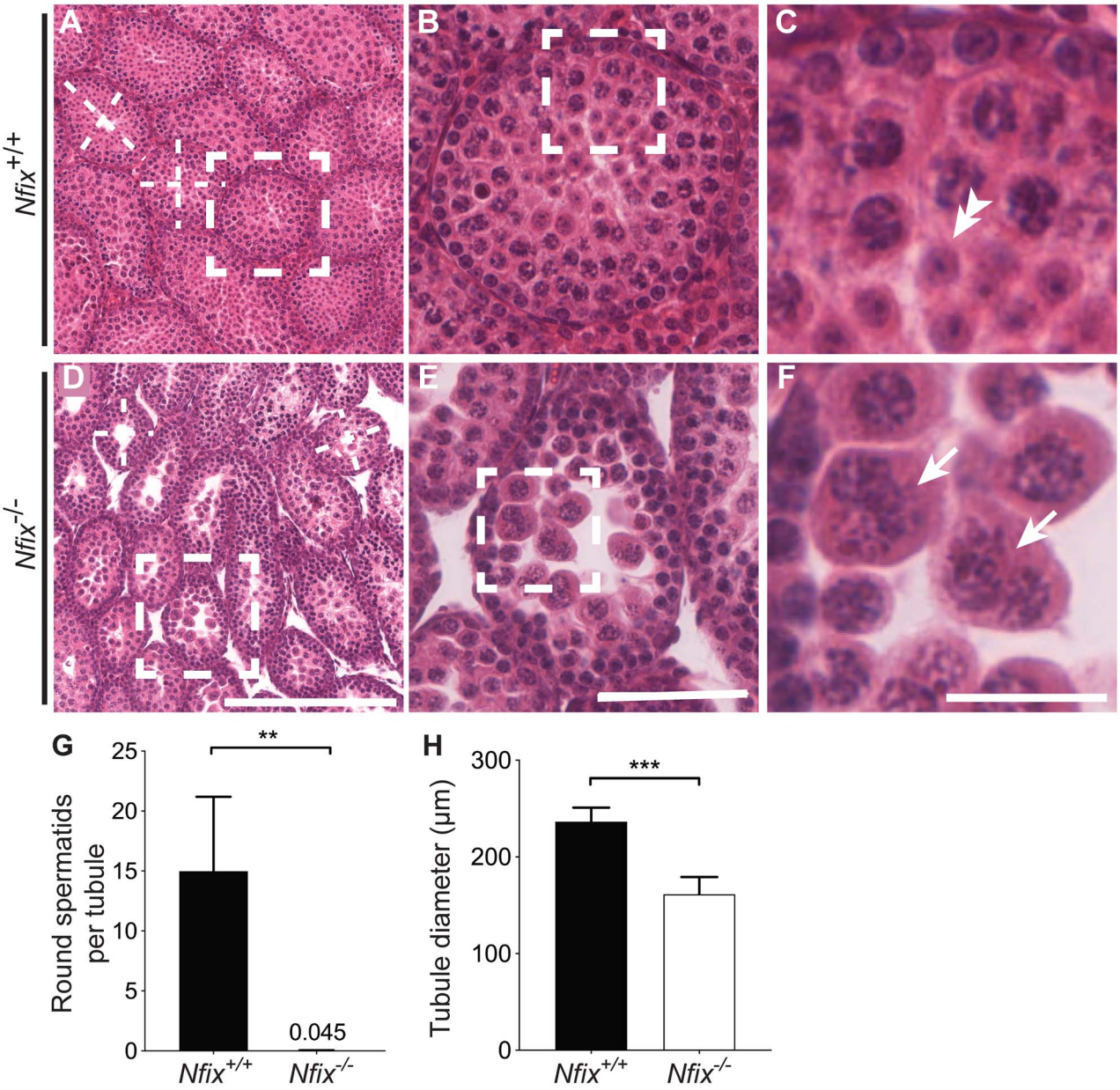

Figure 4. *Nfix* deletion results in germ cell arrest prior to round spermatid formation in the first round of spermatogenesis. Cross sections through testis samples collected from P20 $Nfix^{+/+}$ (*A–C*) and $Nfix^{-/-}$ mice (*D–F*). Paraffin sections were stained with hematoxylin and eosin. The white lines in panels *A* and *C* show the measurements used to calculate the diameter of the seminiferous tubules. Panels *B* and *E* reveal a seminiferous tubule in a wild-type (*B*) and a *Nfix*-null mutant (*E*), respectively; the dashed boxes in these panels are shown in *C* and *F*, respectively. Histological analysis of $Nfix^{+/+}$ mice revealed normal progression through the cycle of the seminiferous epithelium, with round spermatids (double arrowhead in *C*) being the most developed spermatogenic cells present at this age. (*D–F*) In contrast, very few germ cells progressed to round spermatids in the testis of $Nfix^{-/-}$ mice. Moreover, numerous multi-nucleated cells were present in the mutant seminiferous tubule (arrows in *F*). Quantitative analysis showed that $Nfix^{-/-}$ mice had a significant reduction in the number of round spermatids (*G*) and in seminiferous tubule diameter (*H*) in comparison to controls. $n = 4$ for each genotype. Scale bars: *A*, $D = 400\ \mu m$; *B*, $E = 100\ \mu m$; *C*, $F = 50\ \mu m$. Error bars indicate SD, Students *t*-test, $^{**}P < 0.01$, $^{***}P < 0.001$.

Using molecular markers to define the various stages of meiosis I, we found that (i) SYCP3 is mis-localized in some spermatocytes during zygotene; (ii) abnormal multinuclear spermatocytes are produced which is likely linked to the increased levels of apoptosis observed; (iii) although γH2AX localization appears normal, the repair enzyme RAD51 is retained at higher levels, suggesting a failure to successfully repair double-stranded breaks; and (iv) the majority of remaining cells of the germline do not progress further than late pachytene, as very few round spermatids were evident. Because *Nfix*-null mice die by about 20–22 days post-partum, from a range of defects previously detailed by others [29, 42], we were not able to assess the importance of NFIX during adult spermatogenesis.

We observed the abnormal zygotene cells containing large SYCP3-positive clumps or aggregates located next to the nuclear membrane in just over 50% of zygotene-containing tubules at P20. Rare cells with SYCP3 clumping have been noted previously in wild-type rat testes, and this was interpreted as indicative of spermatocytes undergoing apoptosis [43]. Based on this, it is possible that *Nfix* deletion results

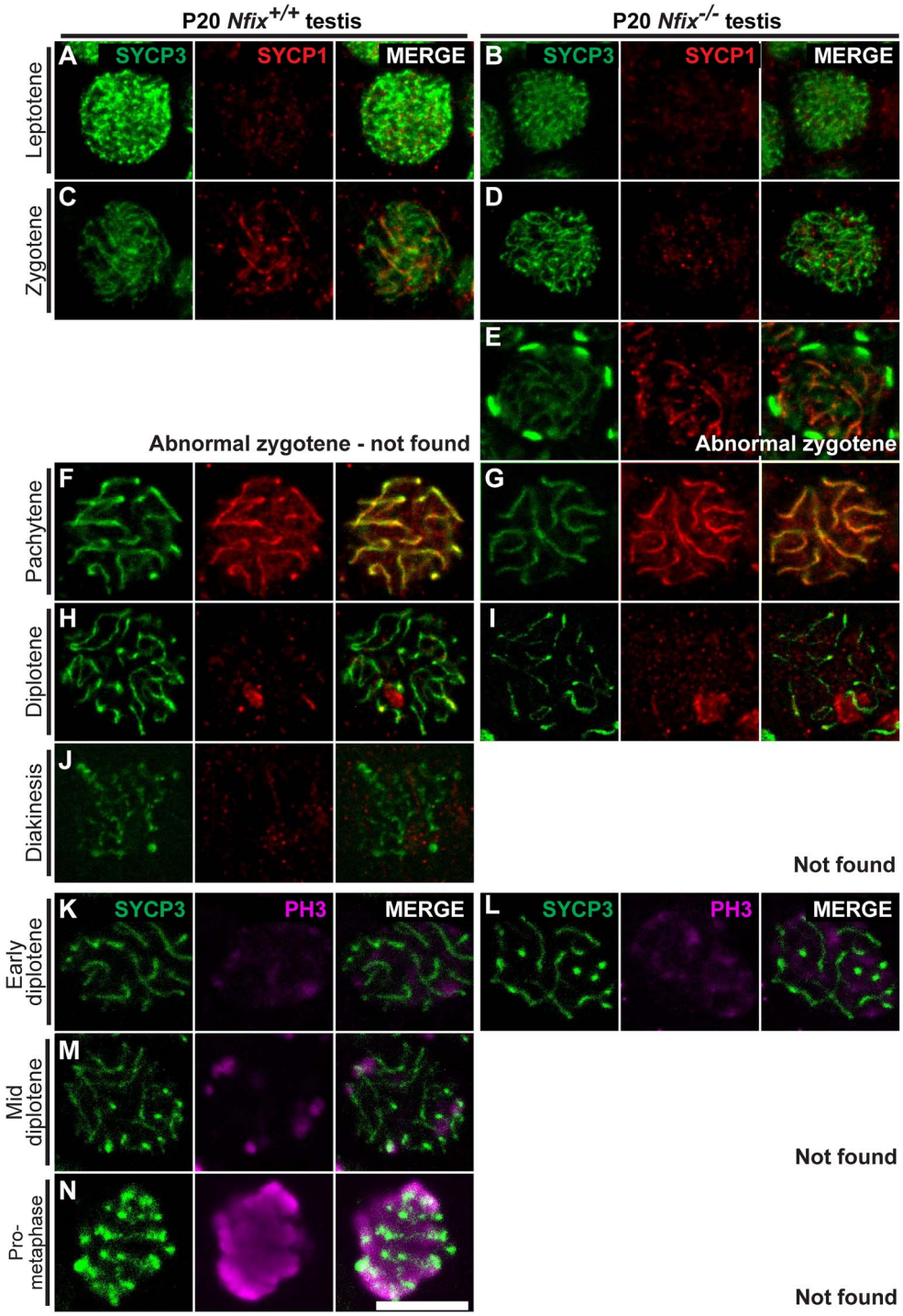

Figure 5. Meiosis is blocked at diplotene stage with defects in the early formation of the synaptonemal complex in *Nfix*-null testes. (*A*–*L*) The progress of prophase I in P20 testes of wild-type (*A*, *C*, *F*, *H*, *J*, *K*, *M*, *N*) and *Nfix*-null (*B*, *D*, *E*, *G*, *I*, *L*) mice was analyzed via the detection of SYCP1 (red) and SYCP3 (green) expression. Extensive networks of fine SYCP3 threads without the SYCP1 protein were observed in leptotene (*A*, *B*), with SYCP1 detected at zygotene in both wild-type and *Nfix*-null samples (*C*, *D*). Some zygotene stage cells in the *Nfix*-null testis exhibited large aggregates of SYCP3 that have not assembled with the synaptonemal complex and appear at the periphery of the nuclear envelope (*E*, observed in approximately 23% of tubules). Pachytene and diplotene spermatocytes had a normal configuration of transverse filaments (SYCP1) and lateral elements (SYCP3) of the synaptonemal complex (*F*, *G*, *H*, *I*). However, although diakinesis was observed in wild-type samples (*J*), no examples of spermatocytes in diakinesis were found in the *Nfix*-null testes. PH3 expression (purple), which is indicative of transition from prophase to metaphase, was observed in the wild-type (*K*) and mutant (*L*) at early diplotene. However, while PH3 expression in the wild-type was observed at mid diplotene (*M*) and pro-metaphase (*N*), it was not observed in the *Nfix* mutant, indicating that meiosis arrests in early diplotene in the absence of NFIX. $n = 3$ for each genotype. Scale bar: 10 μm.

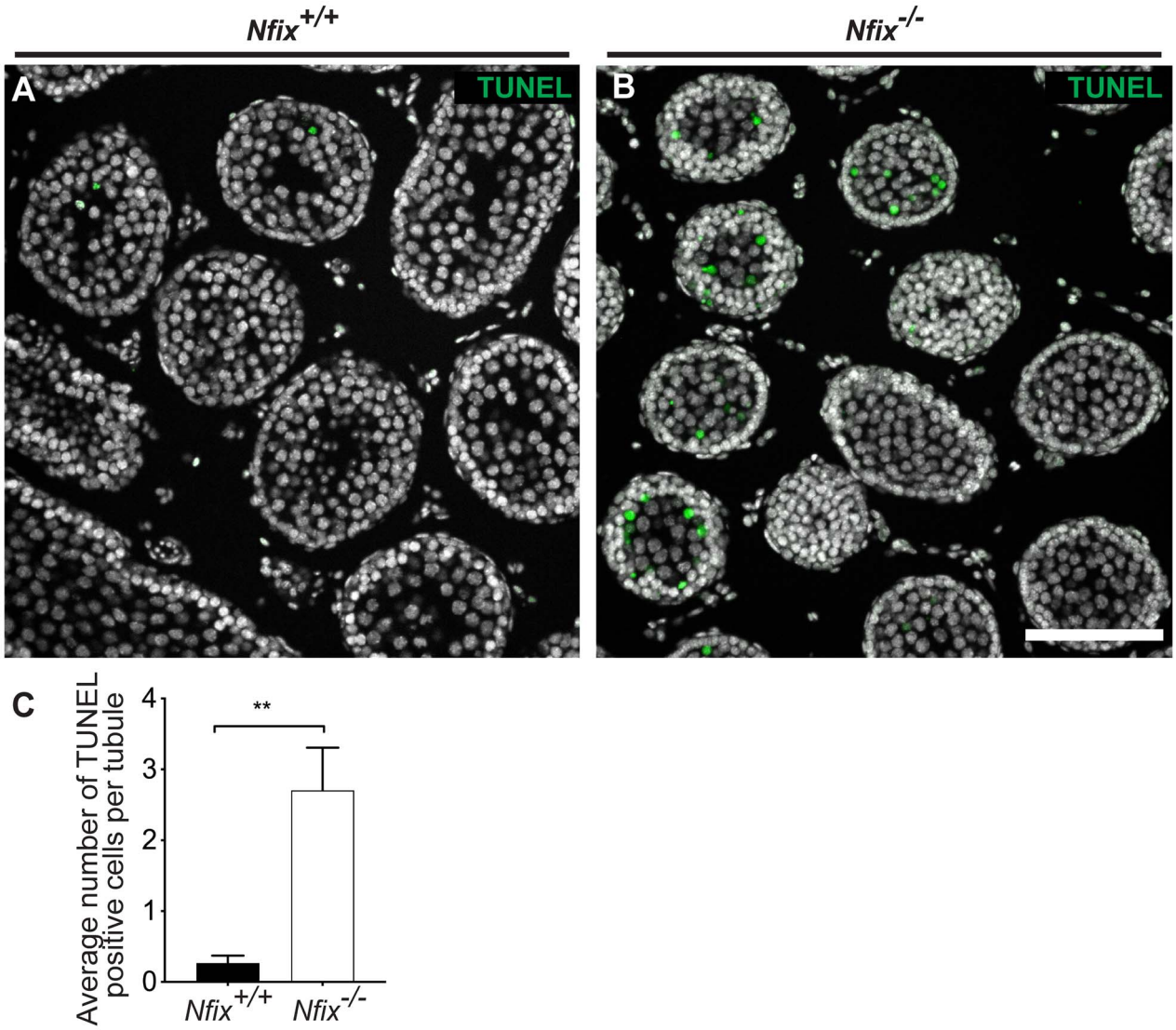

Figure 6. Increased apoptosis in the first wave of spermatogenesis in *Nfix*-null mice. Identification of apoptotic cells in the testis by TUNEL (green) in P20 wild-type (*A*) and *Nfix*-null (*B*) mice. In the control, very few cells were observed undergoing apoptosis (*A*), but the majority of tubules from *Nfix*-null mice contained apoptotic cells (*B*). (*C*) Quantification of TUNEL-positive cells per tubule. We observed that the mean of apoptotic spermatogenic cells in $Nfix^{-/-}$ (2.705) testes was 10 times higher than that in $Nfix^{+/+}$ (0.2692) testes. Scale bar: 100 μm, $n = 3$ for each genotype. Error bars indicate SD, Students *t*-test, $^{**}P < 0.001$.

in germ cell apoptosis, making spermatocytes with obvious SYCP3 clumping more common in mutant testes; alternatively, *Nfix* deletion may lead to mis-localized SYCP3 per se, resulting in activation of the mid-pachytene meiotic checkpoint and apoptosis. It has been reported that the SYCP3 protein can self-assemble [44, 45], so it is possible that *Nfix* deletion results in production of excessive SYCP3 protein which then clumps abnormally. Unlike SYCP3 clumps that are observed in the *Dmc1*-null [46] or *Sycp2*-null [47], the *Nfix*-null clumps are rather regular in appearance and appear to be associated with the nuclear envelope. In our *Nfix*-null model, formation of DSBs appeared normal, as judged by staining for γH2AX; however, we found that RAD51 protein was retained. This might indicate that repair of DSBs is abnormal, or that chromosomal asynapsis is incomplete in the absence of NFIX. Although it has been reported that SYCP3 suppresses the RAD51-mediated strand invasion reaction [48], we do not think that mis-localized SYCP3 is causing retention of RAD51 in our mouse model, because we observed retained RAD51 in the relatively normal looking zygotene cells, as well as in those with abnormal SYCP3 clumps.

Our present study has several limitations, including that our constitutive deleted *Nfix* model cannot provide information regarding a possible cell-autonomous role for NFIX in the germline. Based on analysis of publicly available datasets, *Nfix* transcript expression is not restricted to germ cells during fetal life but is also expressed at high levels in fetal interstitial cells (located outside the testis cords, including fetal Leydig cells) [49] and at low levels in fetal Sertoli cells, both before birth and during the second week after birth (Supplementary Figure S2). Although this does not necessarily mean that NFIX protein is expressed in fetal somatic cells, it is possible that the progression of the first round of spermatogenesis is compromised in part due to somatic defects that arise during fetal and early postnatal life. A second limitation is that we were unable to ascertain whether adult spermatogenesis

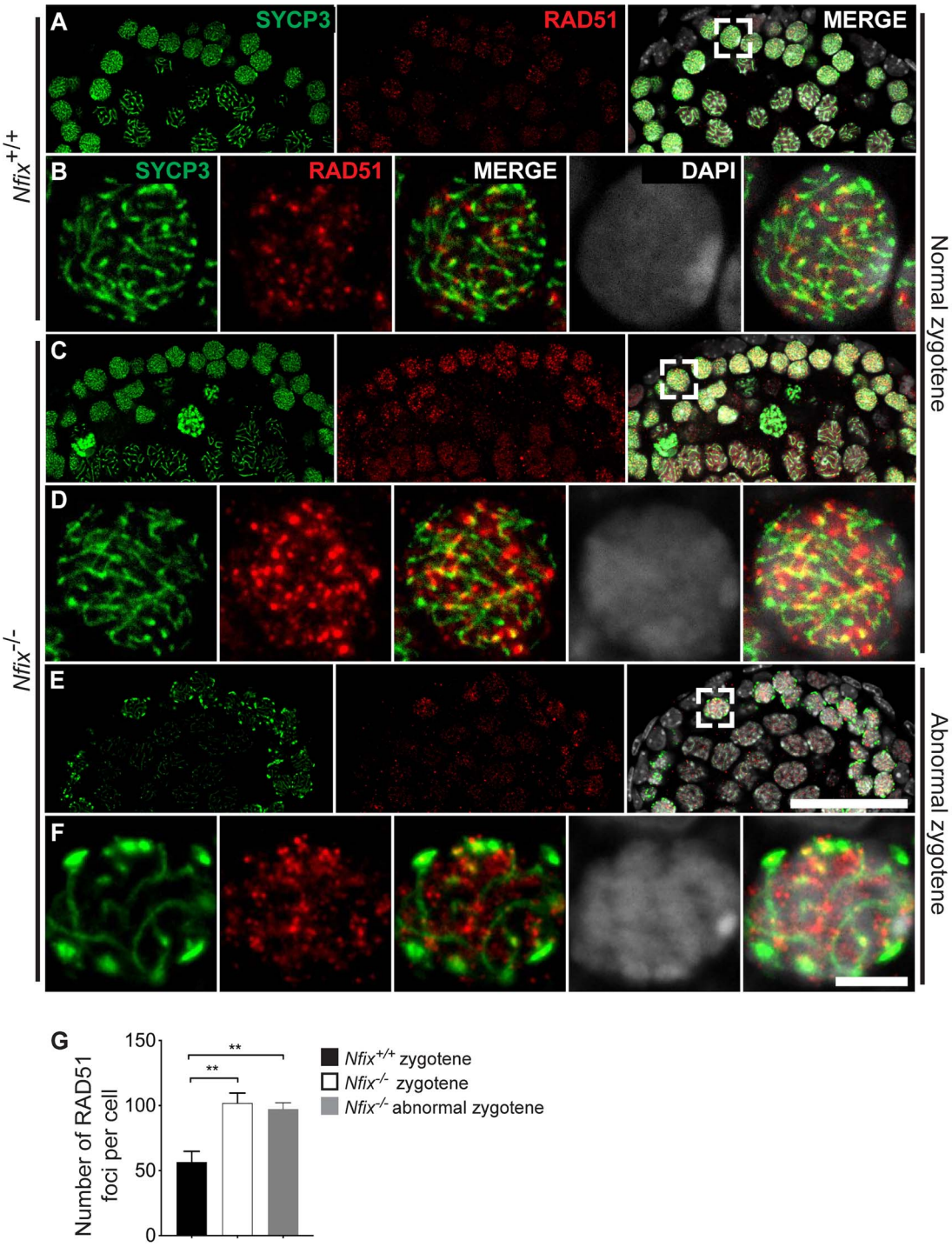

Figure 7. RAD51 foci are retained in late zygotene and pachytene stages in the *Nfix*-null testes. Expression of SYCP3 (green), RAD51 (red), and DAPI (gray) in P20 wild-type (*A, B*) and *Nfix*-null (*C–F*) testes. The dashed boxes in *A, C*, and *E* are shown at higher magnification in *B, D,* and *F,* respectively. Zygotene stage spermatocytes retained more RAD51 foci in the *Nfix*-null testis than in the wild-type (compare the RAD51 expression (red) in *B* and *D*). This was also true for those *Nfix*-null cells with abnormal SYCP3 localization (abnormal zygotene; *E* and *F*). Similarly, RAD51 staining was sparse in pachytene stages of the wild-type (*A*), but remained strong in *Nfix*-null pachytene cells (*C*). (*G*) Quantification of RAD51 foci per cell in zygotene stage from testis of $Nfix^{+/+}$ and $Nfix^{-/-}$ mice. $n = 3$ for each genotype. Scale bars: *A, C, E* = 50 μm, *B, D, F* = 5 μm. Error bars indicate SD, Students *t*-test, $^{**}P < 0.01$.

requires *Nfix*, as the *Nfix*-null mice die at around weaning. Although NFIX was only observed in spermatocytes and not spermatogonia, the very low proportion of SSCs per tubule means that expression in these stem cells cannot be excluded by our analyses. Analysis of steady-state spermatogenesis in pubertal adult and aged mouse testes is required to determine whether NFIX plays a role in SSC biology. Alternatively, it is also possible that only the first, and not subsequent rounds of spermatogenesis, requires NFIX: relevant to this possibility is the fact that the first-round proceeds directly

from pro-spermatogonia, rather than from spermatogonial stem cells [50]. Related to this issue, a third caveat of the *Nfix*-null model is that normal spermatogenic progression may be confounded by the severe growth defect of these mice; nonetheless, formation of highly abnormal-looking zygotene cells suggests that the phenotype we observed in *Nfix*-null testes is not simply due to a spermatogenic delay. Additionally, analysis by [29] revealed one instance of an *Nfix*−/− male surviving to adulthood and being fertile. The morphology of the testis was not examined however, so this does not preclude the possibility of sub-fertility, nor of differences in background strains between the colonies analyzed. All of these issues will be addressed in the future by analysis of mouse model(s) in which *Nfix* is specifically and/or conditionally deleted in the germline.

Our results unlock an exciting new avenue of study. Because NFI proteins are transcription factors, with the potential to influence expression of large cohorts of target genes, it is possible that NFIX and NFIA, in germ cells and Sertoli cells, respectively, play pivotal roles in the regulation of testicular function. Functional or regulatory mutations of *NFIX* would be expected to cause a range of very serious implications in humans and hence are not likely to underlie cases of unexplained male infertility; nonetheless, it will be important to identify the specific targets of NFIX in the context of the postnatal testis as this may substantially increase our understanding of the complex processes of meiosis and spermatogenesis. Recent studies have shown that both NFIX and NFIB regulate open-chromatin domain "super-enhancers," and that ablation of *Nfix* or *Nfib* results in altered accessibility for other transcription factors that, in turn, impacts on lineage fidelity and cellular fate [51]. We are currently preparing cell-specific and conditional deletions of NFIX and NFIA; the unexpected specificity of expression of these two NFI factors within their respective cell types, within the seminiferous tubules, should make comprehensive functional evaluation more tractable than has been the case in other systems.

Materials and methods

Animals and genotyping

This research involved the use of animals. This study was performed with the Australian Code of Practice for the Care and Use of Animals for Scientific Purposes and was carried out with approval from The University of Queensland Institutional Biosafety Committee. The experiments were conducted with approval from the University of Queensland Animal Ethics Committee (AEC approval number QBI/351/16). For analysis of postnatal and adult expression of members of the NFI family, gonadal tissue samples were obtained from the C57BL/6 J wild-type mice. For the analysis of the $Nfix^{-/-}$ (*Nfix*-null) phenotype, samples were obtained from $Nfix^{+/+}$ (wild-type littermates) and $Nfix^{-/-}$ mice maintained on a C57BL/6 J background. The knockout allele excises exon 2, resulting in a premature stop codon, and no NFIX protein is produced [29]. The day of birth was designated as P0. P20 knockout and wild-type and adult wild-type animals were used in this study ($Nfix^{-/-}$ mice die at weaning). The genotype of each mouse was confirmed by polymerase chain reaction (PCR) on DNA prepared from toe samples. The primers used in the reaction amplified a 213 base pair DNA band corresponding to the wild-type *Nfix* allele or a 309 base-pair DNA band corresponding to the *Nfix*-null allele as previously described [29].

Morphological analysis of animal and testis

For comparative analysis of $Nfix^{+/+}$ and $Nfix^{-/-}$ mice, animals were weighed at P20. These mice were also examined visually and photographed. After dissection, testes were weighed, and photographed. All brightfield images of the testes were captured using a Nikon camera (DS-Fi1) at 10× and visualized using ImageJ (National Institutes of Health, Bethesda, MD, USA). Testicular length and width were measured using image analysis software ImageJ.

Tissue collection

The whole testes were dissected from mice immediately after euthanasia. One testis was fixed in Bouin's fixative and the other was fixed in 4% (mass/vol) paraformaldehyde (PFA) overnight at 4 °C. The fixed tissue was dehydrated in various grades of ethanol and finally embedded in paraffin wax blocks.

Histological sectioning and staining

The testes embedded in paraffin were sectioned in a transverse plane at 7-μm thickness using a microtome. Serial sections were mounted on glass slides and dewaxed by immersion into xylene (three times for 5 min) and then rehydrated through an ethanol series (ranging from 100 to 30% ethanol (v/v) in ultrapure (Milli-Q) water). Histological staining of Bouin's fixed samples were performed using hematoxylin and eosin (H&E, Sigma, # HT1101). Brightfield images were captured using a Slide scanner Aperio XT Brightfield (Leica). Immunofluorescence staining used rehydrated samples that had been fixed in 4%PFA/PBS. Slides were submersed in 10-mM citrate buffer (pH 6.0) to perform heat-mediated antigen retrieval, at 95 °C for 15 min. Slides were washed three times for 5 min in PBS/0.1% TX-100 and blocked for 2 h at room temperature in 2% donkey or goat serum and 2% horse serum in PBS (blocking buffer). Primary antibodies were diluted in blocking buffer and applied to slides, incubating overnight at 4 °C. Sections were then washed three times for 5 min with PBS/0.1% TX-100 before the application of appropriate secondary antibodies, diluted in blocking buffer for 2 h. A list of primary antibodies and concentrations used in this study is given in Supplementary Table S1 and secondary antibodies in Supplementary Table S2. Slides were washed as above and counterstained with DAPI for 10 min. Finally, they were mounted in 75% glycerol on Lab-Tek chambered coverglass (Nunc). In attempts to visualize NFIX protein by immunofluorescence, NFIX antibodies ab101341 (Abcam) and NBP2-58904 (Novusbio) raised in rabbit were used without success. The NFIX antibody raised in mouse, listed in Supplementary Table S1, with a different antigen retrieval procedure delivered a positive outcome. The procedure required for NFIX visualization involved microwaving slides in preheated Tris-Based, pH 9, antigen unmasking solution from Vector Labs (LS-J1041-250), for 5 min (power output 550 W). All fluorescent images were captured on an inverted spinning-disk confocal system (Axio Observer Z1 Carl Zeiss; CSU-W1 Yokogawa Corporation of America). The specificity of these anti-NFI antibodies was previously demonstrated using *Nfi*-null tissue [18]. In addition, the secondary antibody without primary antibody (Supplementary Figure S6B) and immunostaining of sections

of *Nfix*-null testes (Supplementary Figure S6C) were used as controls to confirm the specificity of the NFIX antibody.

Image processing and cell counting

Different populations of cells were identified using immunofluorescence with specific cell markers (Supplementary Table S1) or by hematoxylin and eosin using morphological analysis. Sections of testes from $Nfix^{+/+}$ and $Nfix^{-/-}$ mice (minimum $n = 3$ of each genotype) were loaded onto ImageJ (National Institutes of Health, Bethesda, MD, USA), and the cell counter plugin was used to mark and quantify the populations of cells. Levels of colors and brightness were adjusted so that resulting multichannel merged images is aesthetically pleasing. The minimum and maximum limits of displayed range were set identically to all comparable images. To ensure representative counts, the cells were counted from every fifth section from serially sectioned testes (minimum three sections for each testis). Within each testicular section, about 10 seminiferous tubules that were round or nearly round were chosen randomly and measured for each group. The diameter of the seminiferous tubules was also measured as part of the morphometric analysis. The minor and major axes and the mean diameter were obtained. RAD51 foci were counted in zygotene nuclei from at least two cells per section selecting only those foci that were located on the nucleus of the cell. Foci counts was performed in images that were took three consecutive 2-μm-thick optical sections to generate a 6-μm-thick z stack.

Statistical analyses

All statistical analyses of data collected throughout this project were performed using Prism6 software (GraphPad). Two-tailed unpaired Students *t*-tests were performed when comparing two groups. Statistical significance was established at a *P*-value of <0.05. Error bars represent the standard deviation of the mean.

Analysis of scRNA-Seq data

The transcriptomes from different published datasets (Supplementary Table S3) were normalized using the scran package [52]. The quickCluster function was used to pre-cluster cells with similar transcription of genes. Size factors were calculated within each cluster using the computeSumFactors function. The log2-transformed of normalized counts were used for downstream analysis. The developmental age and cell type were obtained from metadata of published data. Gene expression violin plots were produced using R ggplot2 package [53].

Code availability: All custom code used in this work is available at the following GitHub repository: https://github.com/bowleslab/nfiFamily.

Data Availability

The data underlying this article are available in the article and in its online supplementary material.

Authors' Contributions

Conceptualization: R.A.D., C.S., J.B., M.P.; Methodology and analysis: R.A.D., C.S., A.F., G.B., C.H., T.H.; Resources: R.M.G., J.B., M.P.; Writing—original draft: R.A.D.; Writing—review and editing: R.A.D., C.S., P.J., J.B., M.P.; Supervision: C.S., A.F., T.H., J.B., M.P.; Project administration: J.B., M.P.; Funding acquisition: C.S., J.B., M.P.

Supplementary Material

Supplementary material is available at *BIOLRE* online.

Acknowledgment

Imaging was carried out in The School of Biomedical Sciences Microscopy and Imaging Facility. We thank the facility manager, Dr Shaun Walters, for his assistance. We would also like to thank all of the staff at the UQ Biological Resources animal facility for their assistance with colony maintenance.

Conflict of Interest: The authors declare no potential or actual conflicts of interest with respect to the work reported in this article.

References

1. Vander Borght M, Wyns C. Fertility and infertility: definition and epidemiology. *Clin Biochem* 2018; **62**:2–10.
2. Hess RA, Renato de Franca L. Spermatogenesis and cycle of the seminiferous epithelium. *Adv Exp Med Biol* 2008; **636**:1–15.
3. Borg CL, Wolski KM, Gibbs GM, O'Bryan MK. Phenotyping male infertility in the mouse: how to get the most out of a 'non-performer'. *Hum Reprod Update* 2010; **16**:205–224.
4. Piper M, Gronostajski R, Messina G. Nuclear factor one X in development and disease. *Trends Cell Biol* 2019; **29**:20–30.
5. Zenker M, Bunt J, Schanze I, Schanze D, Piper M, Priolo M, Gerkes EH, Gronostajski RM, Richards LJ, Vogt J, *et al*. Variants in nuclear factor I genes influence growth and development. *Am J Med Genet C Semin Med Genet* 2019; **181**:611–626.
6. Heng YH, McLeay RC, Harvey TJ, Smith AG, Barry G, Cato K, Plachez C, Little E, Mason S, Dixon C, *et al*. NFIX regulates neural progenitor cell differentiation during hippocampal morphogenesis. *Cereb Cortex* 2014; **24**:261–279.
7. Piper M, Barry G, Harvey TJ, McLeay R, Smith AG, Harris L, Mason S, Stringer BW, Day BW, Wray NR, *et al*. NFIB-mediated repression of the epigenetic factor Ezh2 regulates cortical development. *J Neurosci* 2014; **34**:2921–2930.
8. Piper M, Barry G, Hawkins J, Mason S, Lindwall C, Little E, Sarkar A, Smith AG, Moldrich RX, Boyle GM, *et al*. NFIA controls telencephalic progenitor cell differentiation through repression of the notch effector Hes1. *J Neurosci* 2010; **30**:9127–9139.
9. Rossi G, Antonini S, Bonfanti C, Monteverde S, Vezzali C, Tajbakhsh S, Cossu G, Messina G. Nfix regulates temporal progression of muscle regeneration through modulation of Myostatin expression. *Cell Rep* 2016; **14**:2238–2249.
10. Gronostajski RM. Roles of the NFI/CTF gene family in transcription and development. *Gene* 2000; **249**:31–45.
11. Kruse U, Sippel AE. The genes for transcription factor nuclear factor I give rise to corresponding splice variants between vertebrate species. *J Mol Biol* 1994a; **238**:860–865.
12. Grabowska MM, Elliott AD, DeGraff DJ, Anderson PD, Anumanthan G, Yamashita H, Sun Q, Friedman DB, Hachey DL, Yu X, *et al*. NFI transcription factors interact with FOXA1 to regulate prostate-specific gene expression. *Mol Endocrinol* 2014; **28**:949–964.
13. Kruse U, Sippel AE. Transcription factor nuclear factor I proteins form stable homo- and heterodimers. *FEBS Lett* 1994b; **348**:46–50.
14. Meisterernst M, Gander I, Rogge L, Winnacker EL. A quantitative analysis of nuclear factor I/DNA interactions. *Nucleic Acids Res* 1988; **16**:4419–4435.
15. Mason S, Piper M, Gronostajski RM, Richards LJ. Nuclear factor one transcription factors in CNS development. *Mol Neurobiol* 2009; **39**:10–23.

16. Barry G, Piper M, Lindwall C, Moldrich R, Mason S, Little E, Sarkar A, Tole S, Gronostajski RM, Richards LJ. Specific glial populations regulate hippocampal morphogenesis. *J Neurosci* 2008; **28**:12328–12340.
17. Harris L, Zalucki O, Gobius I, McDonald H, Osinki J, Harvey TJ, Essebier A, Vidovic D, Gladwyn-Ng I, Burne TH, *et al.* Transcriptional regulation of intermediate progenitor cell generation during hippocampal development. *Development* 2016; **143**:4620–4630.
18. Chen KS, Lim JWC, Richards LJ, Bunt J. The convergent roles of the nuclear factor I transcription factors in development and cancer. *Cancer Lett* 2017; **410**:124–138.
19. Clark BS, Stein-O'Brien GL, Shiau F, Cannon GH, Davis-Marcisak E, Sherman T, Santiago CP, Hoang TV, Rajaii F, James-Esposito RE, *et al.* Single-cell RNA-Seq analysis of retinal development identifies NFI factors as regulating mitotic exit and late-born cell specification. *Neuron* 2019; **102**:1111–1126 e1115.
20. Deneen B, Ho R, Lukaszewicz A, Hochstim CJ, Gronostajski RM, Anderson DJ. The transcription factor NFIA controls the onset of gliogenesis in the developing spinal cord. *Neuron* 2006; **52**: 953–968.
21. Matuzelski E, Bunt J, Harkins D, Lim JWC, Gronostajski RM, Richards LJ, Harris L, Piper M. Transcriptional regulation of Nfix by NFIB drives astrocytic maturation within the developing spinal cord. *Dev Biol* 2017; **432**:286–297.
22. Ding B, Cave JW, Dobner PR, Mullikin-Kilpatrick D, Bartzokis M, Zhu H, Chow CW, Gronostajski RM, Kilpatrick DL. Reciprocal autoregulation by NFI occupancy and ETV1 promotes the developmental expression of dendrite-synapse genes in cerebellar granule neurons. *Mol Biol Cell* 2016; **27**:1488–1499.
23. Zalucki O, Harris L, Harvey TJ, Harkins D, Widagdo J, Oishi S, Matuzelski E, Yong XLH, Schmidt H, Anggono V, *et al.* NFIX-mediated inhibition of neuroblast branching regulates migration within the adult mouse ventricular-subventricular zone. *Cereb Cortex* 2019; **29**:3590–3604.
24. Ernst C, Eling N, Martinez-Jimenez CP, Marioni JC, Odom DT. Staged developmental mapping and X chromosome transcriptional dynamics during mouse spermatogenesis. *Nat Commun* 2019; **10**:1251.
25. Law NC, Oatley MJ, Oatley JM. Developmental kinetics and transcriptome dynamics of stem cell specification in the spermatogenic lineage. *Nat Commun* 2019; **10**:2787.
26. Stevant I, Kuhne F, Greenfield A, Chaboissier MC, Dermitzakis ET, Nef S. Dissecting cell lineage specification and sex fate determination in gonadal somatic cells using single-cell Transcriptomics. *Cell Rep* 2019; **26**:3272–3283 e3273.
27. Oakberg EF. Duration of spermatogenesis in the mouse and timing of stages of the cycle of the seminiferous epithelium. *Am J Anat* 1956; **99**:507–516.
28. Mahadevaiah SK, Turner JM, Baudat F, Rogakou EP, de Boer P, Blanco-Rodriguez J, Jasin M, Keeney S, Bonner WM, Burgoyne PS. Recombinational DNA double-strand breaks in mice precede synapsis. *Nat Genet* 2001; **27**:271–276.
29. Campbell CE, Piper M, Plachez C, Yeh YT, Baizer JS, Osinski JM, Litwack ED, Richards LJ, Gronostajski RM. The transcription factor Nfix is essential for normal brain development. *BMC Dev Biol* 2008; **8**:52.
30. Vidovic D, Harris L, Harvey TJ, Evelyn Heng YH, Smith AG, Osinski J, Hughes J, Thomas P, Gronostajski RM, Bailey TL, *et al.* Expansion of the lateral ventricles and ependymal deficits underlie the hydrocephalus evident in mice lacking the transcription factor NFIX. *Brain Res* 2015; **1616**:71–87.
31. Print CG, Loveland KL, Gibson L, Meehan T, Stylianou A, Wreford N, de Kretser D, Metcalf D, Kontgen F, Adams JM, *et al.* Apoptosis regulator Bcl-w is essential for spermatogenesis but appears otherwise redundant. *Proc Natl Acad Sci* 1998; **95**: 12424–12431.
32. de Vries FA, de Boer E, van den Bosch M, Baarends WM, Ooms M, Yuan L, Liu JG, van Zeeland AA, Heyting C, Pastink A. Mouse Sycp1 functions in synaptonemal complex assembly, meiotic recombination, and XY body formation. *Genes Dev* 2005; **19**:1376–1389.
33. Kolas NK, Yuan L, Hoog C, Heng HH, Marcon E, Moens PB. Male mouse meiotic chromosome cores deficient in structural proteins SYCP3 and SYCP2 align by homology but fail to synapse and have possible impaired specificity of chromatin loop attachment. *Cytogenet Genome Res* 2004; **105**:182–188.
34. Yuan L, Liu J-G, Zhao J, Brundell E, Daneholt B, Höög C. The murine SCP3 gene is required for Synaptonemal complex assembly, chromosome synapsis, and male fertility. *Mol Cell* 2000; **5**:73–83.
35. Fraune J, Schramm S, Alsheimer M, Benavente R. The mammalian synaptonemal complex: protein components, assembly and role in meiotic recombination. *Exp Cell Res* 2012; **318**:1340–1346.
36. Cobb J, Miyaike M, Kikuchi A, Handel MA. Meiotic events at the centromeric heterochromatin: histone H3 phosphorylation, topoisomerase II alpha localization and chromosome condensation. *Chromosoma* 1999; **108**:412–425.
37. Hendzel MJ, Wei Y, Mancini MA, Van Hooser A, Ranalli T, Brinkley BR, Bazett-Jones DP, Allis CD. Mitosis-specific phosphorylation of histone H3 initiates primarily within pericentromeric heterochromatin during G2 and spreads in an ordered fashion coincident with mitotic chromosome condensation. *Chromosoma* 1997; **106**:348–360.
38. Clement TM, Inselman AL, Goulding EH, Willis WD, Eddy EM. Disrupting cyclin dependent kinase 1 in spermatocytes causes late meiotic arrest and infertility in mice. *Biol Reprod* 2015; **93**:137.
39. Neale MJ, Keeney S. Clarifying the mechanics of DNA strand exchange in meiotic recombination. *Nature* 2006; **442**:153–158.
40. Barlow AL, Benson FE, West SC, Hulten MA. Distribution of the Rad51 recombinase in human and mouse spermatocytes. *EMBO J* 1997; **16**:5207–5215.
41. Chaudhry AZ, Lyons GE, Gronostajski RM. Expression patterns of the four nuclear factor I genes during mouse embryogenesis indicate a potential role in development. *Dev Dyn* 1997; **208**: 313–325.
42. Driller K, Pagenstecher A, Uhl M, Omran H, Berlis A, Grunder A, Sippel AE. Nuclear factor I X deficiency causes brain malformation and severe skeletal defects. *Mol Cell Biol* 2007; **27**:3855–3867.
43. Escobar ML, Echeverria OM, Valenzuela YM, Ortiz R, Torres-Ramirez N, Vazquez-Nin GH. Histochemical study of the emergence of apoptosis and altered SYCP3 protein distribution during the first Spermatogenic wave in Wistar rats. *Anat Rec (Hoboken)* 2019; **302**:2082–2092.
44. Syrjanen JL, Pellegrini L, Davies OR. A molecular model for the role of SYCP3 in meiotic chromosome organisation. *elife* 2014; **3**:e02963.
45. Yuan L, Pelttari J, Brundell E, Bjorkroth B, Zhao J, Liu JG, Brismar H, Daneholt B, Hoog C. The synaptonemal complex protein SCP3 can form multistranded, cross-striated fibers in vivo. *J Cell Biol* 1998; **142**:331–339.
46. Pittman DL, Cobb J, Schimenti KJ, Wilson LA, Cooper DM, Brignull E, Handel MA, Schimenti JC. Meiotic prophase arrest with failure of chromosome synapsis in mice deficient for Dmc1, a germline-specific RecA homolog. *Mol Cell* 1998; **1**:697–705.
47. Yang F, De La Fuente R, Leu NA, Baumann C, McLaughlin KJ, Wang PJ. Mouse SYCP2 is required for synaptonemal complex assembly and chromosomal synapsis during male meiosis. *J Cell Biol* 2006; **173**:497–507.
48. Kobayashi W, Hosoya N, Machida S, Miyagawa K, Kurumizaka H. SYCP3 regulates strand invasion activities of RAD51 and DMC1. *Genes Cells* 2017; **22**:799–809.
49. Jameson SA, Natarajan A, Cool J, DeFalco T, Maatouk DM, Mork L, Munger SC, Capel B. Temporal transcriptional profiling of somatic and germ cells reveals biased lineage priming of sexual fate in the fetal mouse gonad. *PLoS Genet* 2012; **8**:e1002575.
50. Yoshida S, Sukeno M, Nakagawa T, Ohbo K, Nagamatsu G, Suda T, Nabeshima Y. The first round of mouse spermatogenesis is a distinctive program that lacks the self-renewing spermatogonia stage. *Development* 2006; **133**:1495–1505.

51. Adam RC, Yang H, Ge Y, Infarinato NR, Gur-Cohen S, Miao Y, Wang P, Zhao Y, Lu CP, Kim JE, *et al.* NFI transcription factors provide chromatin access to maintain stem cell identity while preventing unintended lineage fate choices. *Nat Cell Biol* 2020; **22**:640–650.
52. Lun AT, Bach K, Marioni JC. Pooling across cells to normalize single-cell RNA sequencing data with many zero counts. *Genome Biol* 2016; **17**:75.
53. Hintze JL, Nelson RD. Violin plots: a box plot-density trace synergism. *Am Stat* 1998; **52**:181–184.